The North Atlantic Oscillation, Surface Current Velocities, and SST Changes in the Subpolar North Atlantic

MARIA K. FLATAU,* LYNNE TALLEY, AND PEARN P. NIILER

Scripps Institution of Oceanography, University of California, San Diego, La Jolla, California

(Manuscript received 24 April 2002, in final form 30 January 2003)

ABSTRACT

Changes in surface circulation in the subpolar North Atlantic are documented for the recent interannual switch in the North Atlantic Oscillation (NAO) index from positive values in the early 1990s to negative values in 1995/96. Data from Lagrangian drifters, which were deployed in the North Atlantic from 1992 to 1998, were used to compute the mean and varying surface currents. NCEP winds were used to calculate the Ekman component, allowing isolation of the geostrophic currents. The mean Ekman velocities are considerably smaller than the mean total velocities that resemble historical analyses. The northeastward flow of the North Atlantic Current is organized into three strong cores associated with topography: along the eastern boundary in Rockall Trough, in the Iceland Basin (the subpolar front), and on the western flank of the Reykjanes Ridge (Irminger Current). The last is isolated in this Eulerian mean from the rest of the North Atlantic Current by a region of weak velocities on the east side of the Reykjanes Ridge.

The drifter results during the two different NAO periods are compared with geostrophic flow changes calculated from the NASA/Pathfinder monthly gridded sea surface height (SSH) variability products and the Advanced Very High Resolution Radiometer (AVHRR) SST data. During the positive NAO years the northeastward flow in the North Atlantic Current appeared stronger and the circulation in the cyclonic gyre in the Irminger Basin became more intense. This was consistent with the geostrophic velocities calculated from altimetry data and surface temperature changes from AVHRR SST data, which show that during the positive NAO years, with stronger westerlies, the subpolar front was sharper and located farther east. SST gradients intensified in the North Atlantic Current, Irminger Basin, and east of the Shetland Islands during the positive NAO phase, associated with stronger currents. SST differences between positive and negative NAO years were consistent with changes in air–sea heat flux and the eastward shift of the subpolar front. SST advection, as diagnosed from the drifters, likely acted to reduce the SST differences.

1. Introduction

This paper investigates the changes in the ocean surface circulation in the subpolar North Atlantic associated with the interannual ''switch'' in the North Atlantic Oscillation (NAO) pattern from positive in the early 1990s to negative in the fall of 1995/96. As a part of this investigation, the mean surface circulation is also derived using surface drifter data and the anomalous circulation from drifters is compared with that from altimetry.

The NAO is a major component of interannual to interdecadal variability in the North Atlantic area. Its atmospheric component is characterized by a sea level pressure (SLP) dipole between the Icelandic low and Bermuda high. Recently, Thompson et al. (2000) postulated that the NAO is a part of the more general Arctic Oscillation (AO) pattern. The AO can be viewed as a zonally symmetric ''seesaw'' in the atmospheric mass over the polar cap and midlatitude zonal ring centered around 45°N and is related to the strength of the stratospheric polar vortex. In this interpretation the zonally symmetric part of NAO is related to the AO state and the zonal asymmetries result from the land–sea contrast. While the NAO index is usually based on the local SLP difference between Iceland and Portugal, the AO state is defined by the leading mode empirical orthogonal function of the monthly mean surface pressure north of 25°N (Thompson and Wallace 1998). In the North Atlantic the ''high index'' NAO and AO are characterized by a larger meridional pressure gradient, stronger westerlies, and northeastward displacement of the storm track compared with a low index. The SST pattern that accompanies the positive NAO regime has a structure with low temperatures in the polar regions and south of 20°N, and higher SSTs between 25° and 45°N.

The causes of the AO or NAO variability and the role

* Current affiliation: Naval Research Laboratory, Monterey, California.

Corresponding author address: Dr. Lynne D. Talley, Scripps Institution of Oceanography, University of California, San Diego, 9500 Gilman Dr., La Jolla, CA 92093-0230.
E-mail: ltalley@ucsd.edu

© 2003 American Meteorological Society

of the ocean are subject to vigorous investigation. Observations indicate that the midlatitude ocean responds to the surface flux anomalies created by an atmospheric circulation related to the NAO (Cayan 1992). Joyce et al. (2000) observed the changes in the Subtropical Mode Water (STMW) related to atmospheric buoyancy fluxes and hypothesized that a north–south shift of the Gulf Stream position associated with STMW modification could influence the midlatitude storms in the atmosphere and lead to a coupled oscillation. There is also evidence (Sutton and Allen 1997) that the SST anomalies forced by atmospheric circulation can propagate along the the Gulf Stream and the North Atlantic Current, influencing the temperature in the North Atlantic about 7 yr after their forcing by the original atmospheric disturbance.

Forcing of the atmosphere by the ocean is harder to observe. Nevertheless, Czaja and Frankignoul (1999) in their analysis of the covariance between atmospheric circulation and SST anomalies in the North Atlantic show maximum covariance at a 6-month lag (SST leading the atmospheric circulation). They suggest that the anomalous tropospheric circulation is driven by the anomalous heat flux related to SST. Observations of ice cover in the Arctic (Mysak and Venegas 1998) show that fluctuation of ice extent can also contribute to changes in the atmospheric pressure and NAO pattern by influencing the surface heat flux.

In general, the ocean–atmosphere coupling mechanism may involve the generation of the SST–ocean circulation anomaly by atmospheric anomalies, advection of anomalous SST by the ocean currents, or triggering the anomalous SST pattern by anomalous circulation and response of the atmosphere to the new anomalous SST field. Because of all the processes involved, the description of anomalous ocean currents related to NAO variability is quite important.

The recent switch in the NAO index that occurred in 1995 was during a period of intense in situ ocean observations and global satellite coverage. This created the opportunity for extensive documentation of atmospheric and oceanic changes related to the NAO pattern reversal. Using data from a World Ocean Circulation Experiment (WOCE) hydrographic section between Greenland and Ireland, Bersch et al. (1999) noticed that relaxation of the NAO positive phase in 1995/96 was accompanied by decreased density in the Subpolar Mode Water, westward retreat of the subpolar front in the Iceland Basin, and suppressed spreading of the Labrador Sea Water. Reverdin et al. (1999) documented the changes in ocean temperature along line AX2 of WOCE (between Iceland and Newfoundland). They noticed that interannual changes observed between 1994 and 1998 were larger than the seasonal cycle. They concluded that although there was a strong correlation between the heat fluxes and temperature variability, not all the heat content change observed during this time could result from air–sea heat fluxes, and some other processes contributed to the heating observed after 1996.

The goal of this work is to assess the change in surface currents associated with the relaxing of positive NAO at the end of 1995. The area of interest is shown in Fig. 1. Our primary dataset is the Lagrangian drifters deployed in the Atlantic between 1992 and 1998. Much of this dataset was included in the analysis by Fratantoni (2001) of Lagrangian drifters from the 1990s. Our analysis provides more uniform gridded coverage, particularly of the northeast Atlantic and regions of low velocity, and also includes a separation into the Ekman and non-Ekman (essentially geostrophic) flows. The National Centers for Environmental Prediction (NCEP) winds were used to compute Ekman velocities, yielding an estimate of the geostrophic flow field based on the drifters. The circulation changes inferred from the drifters were compared to the geostrophic flow anomalies calculated from satellite altimetry data and the temperature anomalies were obtained from the Jet Propulsion Laboratory (JPL) Advanced Very High Resolution Radiometer (AVHRR) weekly averaged, gridded SST. NCEP reanalysis data were used to asses the surface fluxes.

2. Atmospheric circulation patterns in 1992–98

The North Atlantic Oscillation index between 1992 and 1998 used in this paper was taken from NCEP. The NCEP index is based on principal component analysis of the most prominent teleconnection patterns (Barnston and Livezey 1987) and is calculated monthly. We defined the state of the NAO using the value of this index averaged for the winter months (December to February; Fig. 2). The NAO index defined in this manner was predominantly positive in the 1990s following the trend that started in the 1980s. However, a short period of reversal occurred between 1995 and 1998, when the index suddenly switched from a high positive value (0.9) in the winter of 1994/95 to a low value (-0.4) the following winter. In 1996/97 the index increased but remained negative, and decreased again in 1997/98. The positive NAO phase returned in winter 1998/99. The value of the index changed slightly if March or March and April were included in the average, but the essential characteristics of the NAO evolution, with the 1995/96 switch and ensuring weaker but negative NAO, remained the same.

A single-variable NAO index, based on the pressure difference between Lisbon, Portugal, and southwest Iceland (Hurrell 1995), showed a slightly different temporal pattern. In became negative in 1995/96, but positive (although small) values returned in the two following years. The large positive values appeared again in 1998/99. Also, even for the NCEP index, including March in the calculation of the winter average makes winter index values after 1994/95 close to zero instead of negative. However, it will be shown later in the paper that the atmospheric and oceanic circulation showed the characteristics of the negative NAO not only in 1996,

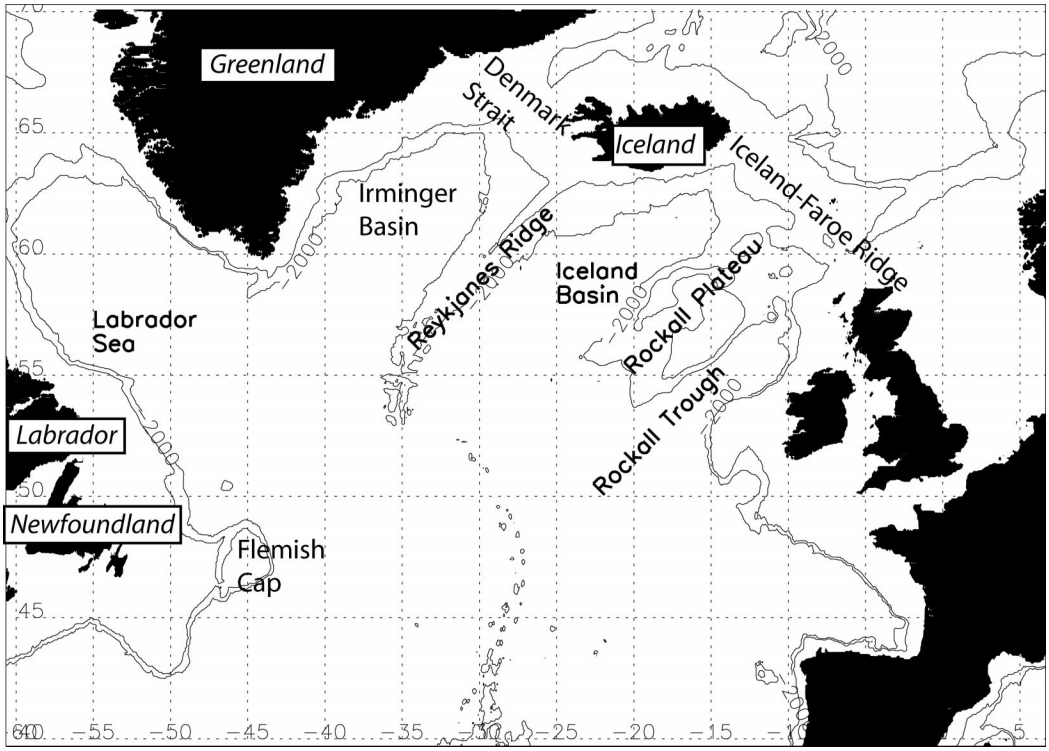

FIG. 1. The subpolar North Atlantic.

but also in the two following years. Therefore, as indicated by the index based on principal component analysis, 1992/93, 1993/94, and 1994/95 will be referred to as positive NAO winters, and 1995/96, 1996/97, and 1997/98 as negative NAO winters.

The weakening of the Icelandic low in the winter of 1995/96 caused a decrease of the midlatitude westerlies that continued into the two following winters. As shown in Fig. 3, in the positive NAO years the westerlies were stronger and persisted throughout the whole winter, while during the years that followed the switch, strong westerly wind was present only sporadically.

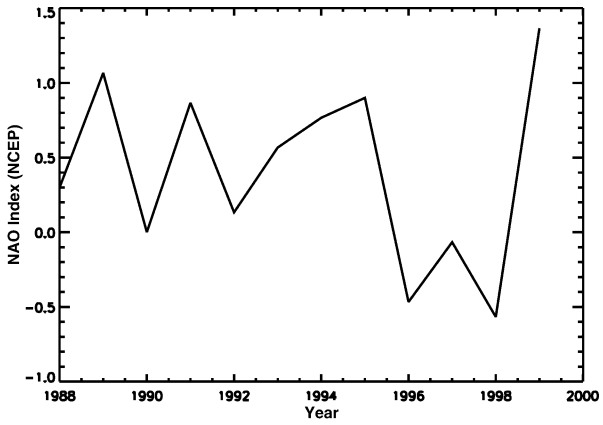

FIG. 2. Winter (Dec–Jan–Feb) NAO index for 1988–99 (from the NCEP analysis of teleconnection patterns).

The map of the difference between winter (December–February) wind stress for the NAO positive and negative years (Fig. 4a) indicates that the magnitude of stress was larger during the positive NAO years for most of the North Atlantic, with the exception of a small region southeast of Iceland. Positive NAO winters were characterized by stronger westerlies, with maximum values of about 0.15 N m^{-2} and large northerlies (0.3 N m^{-2}) along the Greenland coast, especially between 70°, and 75°N, consistent with the surface pressure anomaly (not shown here).

3. The influence of the NAO status on surface circulation

a. The average surface circulation

From 1992 to 1998, data from 687 drifting buoys were available for the North Atlantic. This excellent coverage allowed us to calculate the mean surface currents and evaluate the variability of the circulation associated with changing NAO forcing. This drifter dataset was used by Fratantoni (2001), who emphasized the regions of especially large velocities, with regional analyses of the Gulf Stream and North Atlantic Current, the Labrador Sea, and the Caribbean. Our mean flow differs in some respects from Fratantoni's, but we emphasize that our analysis is focused on the variations in circulation associated with the NAO.

The drifter dataset used in this paper consists of drifter

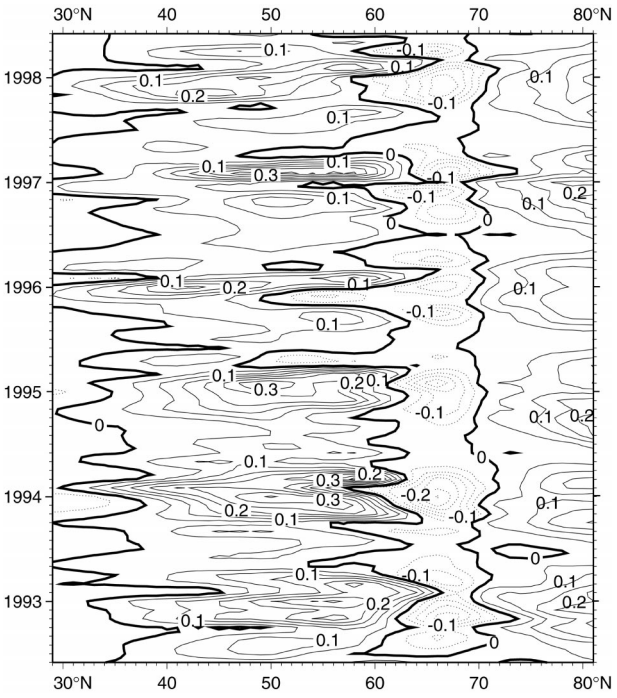

FIG. 3. Time–latitude diagram of the zonal wind stress (N m^{-2}) from NCEP reanalysis monthly data, for the period covered by the drifter dataset. The values are averaged in the longitude band from 50° to 10°W. Dashed contours are negative values.

positions and velocities interpolated in time by krigeing to four data points per day, both by the Atlantic Oceanographic and Meteorological Laboratory (AOML) Drifter Data Center (Hansen and Poulain 1996). The data also included NCEP surface wind velocities interpolated to each drifter's position. The interpolated surface winds were used to correct the drifter velocities for the slippage caused by the wind as described in Pazan and Niiler (2001).

The average surface flow and error ellipses calculated from the complete dataset are shown in Fig. 5. The error ellipses are estimated assuming that the decorrelation time is 5 days (McClean et al. 2002). Figure 5 indicates that in the area of strong currents such as the East and West Greenland Currents, the Labrador Current, the North Atlantic Current, or the cyclonic gyre in the Irminger Basin, the errors are fairly small compared to the magnitude of the flow. The largest errors are in the centers of the basins (Labrador Sea, Irminger and Iceland Basins) and over Rockall Plateau, where the mean flow is small. Large errors are also present close to the coasts where only a small number of drifters were present. Analysis of individual drifter tracks indicates that south of Iceland, the large errors compared to the magnitude of mean flow result not from limited sampling, but from the presence of mesoscale vortices.

The data were further processed to calculate seasonal and interannual variability, and to calculate the mean Ekman and a representation of the mean geostrophic velocity. The velocities for each drifter were smoothed using a 5-day running mean filter. The data were binned in $1° \times 1°$ bins, and monthly averages of drifter velocities were calculated for each bin. NCEP wind stresses were interpolated to each drifter position and time. These winds were binned and averaged for each month as for drifter velocities, and were then used to calculate the monthly averaged Ekman velocity in each bin, using the model developed in Ralph and Niiler (1999). These Ekman velocities were then subtracted from the total monthly averaged velocities to obtain the geostrophic circulation. The residual flow is assumed to represent the geostrophic flow, although we have not constrained the circulation to be nondivergent. Although the Ekman model likely has some error, the total Ekman flow is much smaller than the total flow in most regions, and so the geostrophic component should be reasonable.

The average geostrophic flow obtained from the data processed in this manner and the Ekman velocity obtained following the drifter tracks are shown in Fig. 6. The total velocity calculated from the monthly averages (that is the sum of the fields in Figs. 6a,b) is almost identical to the flow obtained by averaging the velocities of all the drifters shown in the previous figure (Fig. 5) and is not shown here. Differences arise primarily where no average vector is reported in Fig. 5 due to a low number of observations for the average (e.g., the East Greenland Current north of Denmark Strait).

The Ekman mean flow so constructed constitutes only a small fraction of the total velocity of the drifters. The Ekman flow is strongest and southeastward in the central North Atlantic between 50° and 55°N, in the region of maximum wind speed. The average Ekman speed is 1.4 cm s^{-1} and the maximum is 6.0 cm s^{-1} at 53°N, 11°W. The largest ratio of Ekman to geostrophic velocity occurs in the regions where the total flow is weak, such as over the Reykjanes Ridge, in the center of the Labrador Sea, and southwest of Iceland. The Ekman drift shown in Fig. 6b closely resembles the drift calculated directly from the NCEP winds at each grid point (not shown here). The largest discrepancies are found north and east of Iceland, near the Labrador coast, and near the coast of the United Kingdom, where the number of drifter data points is relatively small. This reasonable assessment of average Ekman flow from the winds at each drifters' location suggests that in most of the basin the drifter sampling density is adequate to estimate the average total flow. Since the winds in this region are highly variable, we can expect that this drifter sampling density is also sufficient to estimate most of the characteristics of the surface circulation in the ocean.

The mean total velocities and mean geostrophic velocities are similar because of the small Ekman velocities. The surface circulation of the subpolar North Atlantic has been thoroughly described based on dynamic topography in numerous textbooks and publications (Sverdrup et al. 1942; Dietrich et al. 1975; Stommel et al. 1978; Olbers et al. 1985; Krauss 1986; Schmitz and

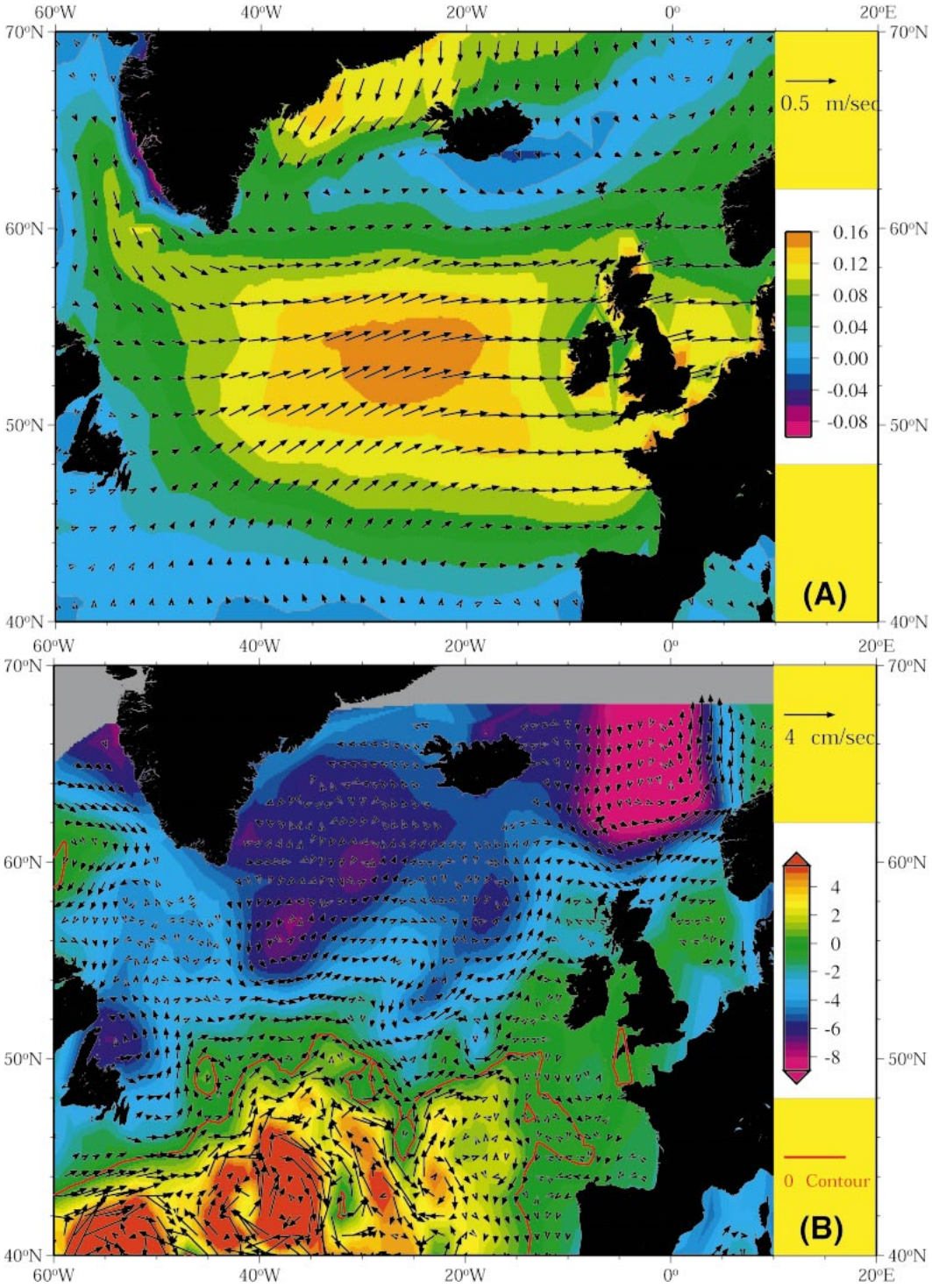

FIG. 4. (a) Positive NAO winter wind stress (1992/93, 1993/94, 1994/95) minus negative NAO winter wind stress (1995/96, 1996/97, 1997/98), where winter is Dec–Feb (shaded). Units are N m^{-2}. Data are from the NCEP reanalysis. The vector difference is shown by arrows and the amplitude of the difference is contoured. (b) SSH (shading; cm) and geostrophic surface current (vectors; cm s^{-1}) for positive NAO minus negative NAO years, based on altimetry observations. Winter–spring (Dec–May) data only.

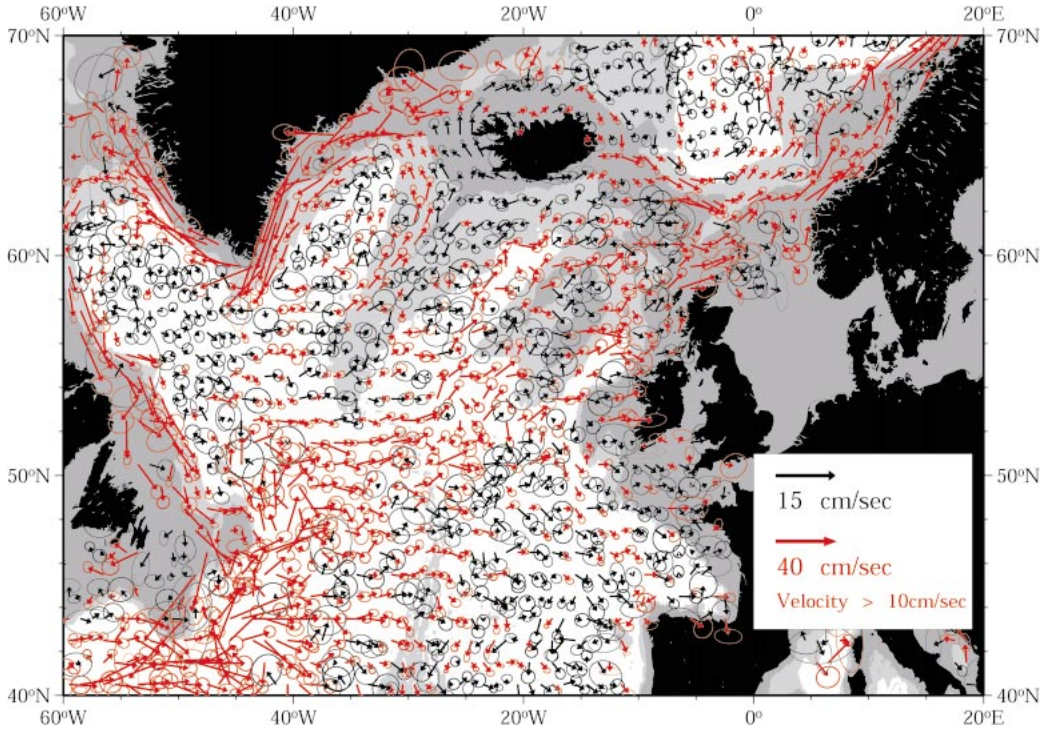

FIG. 5. The mean flow and error ellipses (cm s^{-1}), from the Lagrangian buoys in the North Atlantic using all data from 1992 to 1998. Shading indicates the 1000- and 2500-m bathymetric contours.

McCartney 1993; Reid 1994). Velocities measured using drifters and current meters are the basis for more modern surface circulation analyses (Krauss 1986, 1995; Poulain et al. 1996; Orvik et al. 2001; Fratantoni 2001). The mean circulation calculated here from the complete drifter dataset is as comprehensive as any surface circulation produced.

The following surface circulation features are apparent in Fig. 6, proceeding counterclockwise around the map: Gulf Stream (strong eastward flow centered at 40°N west of 50°W); North Atlantic Current (strong western boundary current east of the Grand Banks and Flemish Cap, the eastward flow across the central Atlantic, and the northeastward flow in the eastern Atlantic as far north as the Iceland–Faeroe Ridge with several strong current cores); Iceland–Faeroe Front (strong eastward flow along the Iceland–Faeroe Ridge); Norwegian Current (double-branched eastern boundary flow north of the Iceland–Faeroe Ridge); the North Icelandic Current (northward flow at the west coast of Iceland turning into the eastward flow on the north coast of Iceland, also referred to as the North Icelandic Irminger Current); the East Greenland Current (southward flow along the east coast of Greenland); the West Greenland Current (northward flow along the west coast of Greenland); and the Labrador Current (southward flow along the Labrador coast, extending southward inshore of the northward North Atlantic Current along Newfoundland). The eastward and northeastward portions of the North Atlantic Current (NAC) have also been referred to as the North Atlantic Drift and Northeast Atlantic Current. The subpolar or subarctic front is embedded in the northeastward portion of the North Atlantic Current, and is roughly coincident with the NAC branch in the Iceland Basin.

The northeastern portion of the NAC has three separate regions of intensified northward flow in the Eulerian mean. The easternmost is at the eastern boundary and in Rockall Trough, with an eastern boundary bifurcation into northward and southward flow at 51°N, which is slightly south of the landfall of the zero of the mean wind stress curl. A second locus of intensified northeastward flow is located in the Iceland Basin, west of Rockall Plateau. Somewhat weaker northeastward flow occurs over Rockall Plateau. Thus the NAC forms two strong branches around Rockall Plateau with weak flow in between, similar to the branching of the Norwegian Current around Voring Plateau observed with drifters (Poulain et al. 1996). All of this northeastward flow of the Eulerian mean NAC apparently feeds the Iceland–Faeroe Front and, hence, the Norwegian Current.

The third branch of the NAC is the Irminger Current. It lies over the western flank of the Reykjanes Ridge, and is isolated from these two northeastern Atlantic branches in this Eulerian mean. This branch splits into two at Iceland: one branch that flows around Iceland, becoming the North Icelandic Current, which flows into

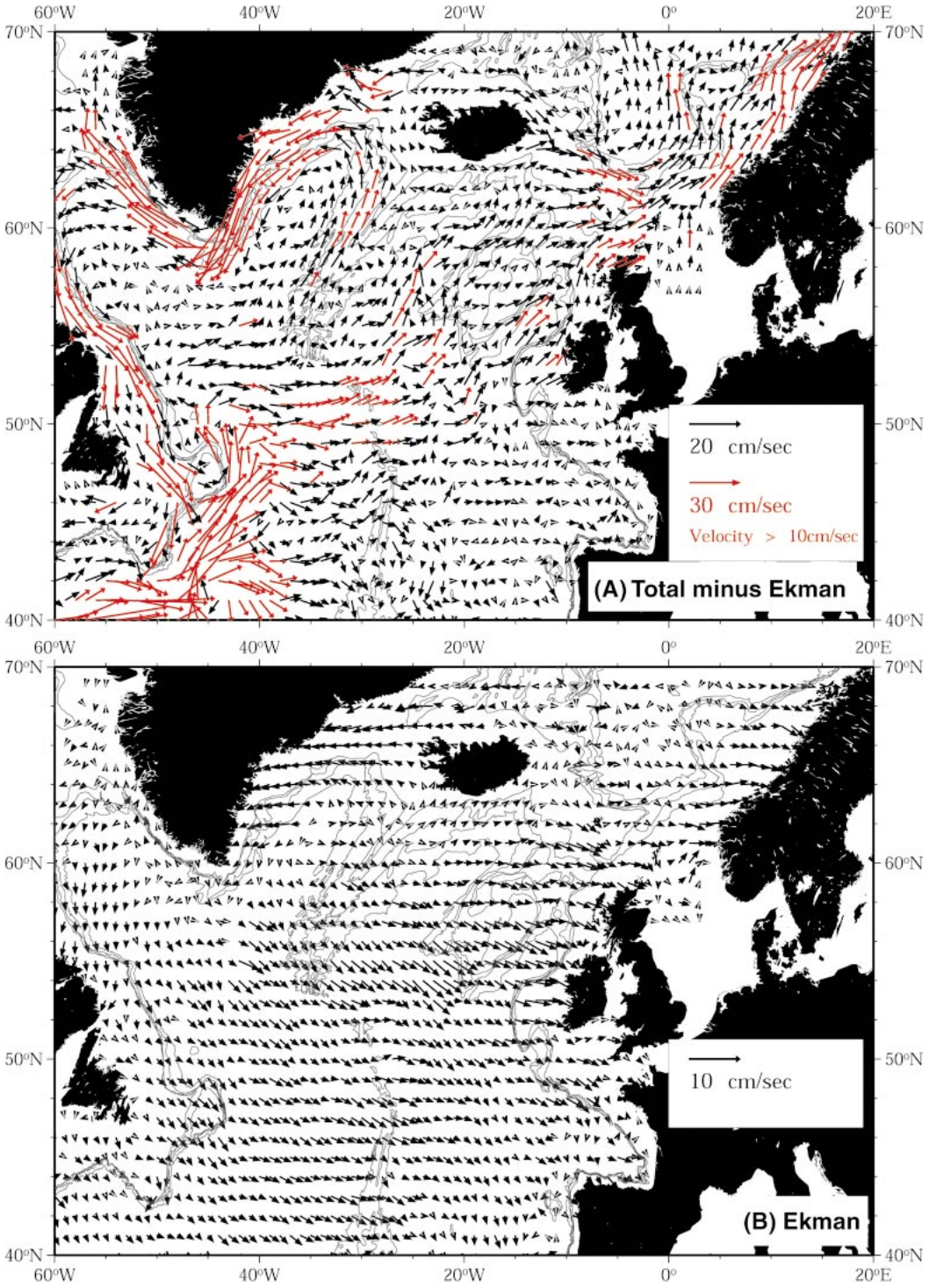

FIG. 6. (a) Average surface geostrophic velocity (cm s^{-1}), based on drifter velocities with Ekman velocities removed (1992–98). (b) Ekman velocity for the same period.

the Iceland–Faeroe Front and then into the Norwegian Current, and a second branch that turns west into the East Greenland Current. In Figs. 5 and 6a, this strong Irminger Current appears connected with the northernmost part of the NAC, which turns eastward in the northwest loop at the mouth of the Labrador Sea. It also appears to be fed internally within the Irminger Basin by the cyclonic circulation within this small basin,

which is born out by individual drifter tracks. A nearly quiescent pool of water lies above the eastern flank of the Reykjanes Ridge, separating the Irminger and Iceland Basin branches of the NAC. Here the Ekman and geostrophic portions of the flow are of nearly the same magnitude, leading to a small net southward flow at some grid points.

The Lagrangian picture of the Irminger Current is somewhat different from Figs. 5 and 6a. The drifter tracks that produce the large velocities over the Reykjanes Ridge originate mostly from either the cyclonic circulation within the Irminger Basin (as in the Eulerian mean) or in the Iceland Basin branch of the NAC, and not from the northwest loop of the NAC (not as in the Eulerian mean). The path from the Iceland Basin branch is muddled by the weak and sometimes southward flows over the east flank of the Reykjanes Ridge, with at least two drifters moving westward around the southern tip of the Reykjanes Ridge similarly to the subsurface (700 m) floats described in Lavender et al. (2000) and Bower et al. (2002). The very weak southward velocities related to this flow can be seen on the eastern side of the Reykjanes Ridge in Fig. 6. The robust feature of both the Eulerian and Lagrangian views is the cyclonic gyre in the Irminger Basin, and we frequently refer to this feature, rather than to the Irminger Current per se.

Examination of drifter tracks elsewhere in the subpolar region indicates that the drifters in the intense northward branches of the NAC in the Iceland Basin and Rockall Trough originate in the Labrador Sea and cross the Atlantic at about 50°N. No drifters from the Gulf Stream (intense eastward flows in the southwest corner of Figs. 5 and 6b) crossed into the NAC and subpolar gyre.

b. NAO+/NAO− circulation and SSH changes based on altimetry

We examine the evolution of surface currents from 1993 to 1998 using the drifter data described in the previous section and the sea surface height (SSH) data from the National Aeronautics and Space Administration (NASA) Ocean Altimeter Pathfinder Project monthly gridded SSH variability products. The altimetry dataset has more comprehensive spatial coverage with uniform sampling than the drifter data, and so is the first product described here. In comparing drifter and altimetric results in the next section, we find that the drifter coverage is good in most regions and also that the altimetric velocities are underestimated by a factor of 2–3 because of the larger spatial scale of the necessarily smoothed data altimetric set.

The altimetric SSH data consist of variations with respect to the 1993 mean surface, and have been generated from all available altimeter observations (*Seasat, Geosat, ERS-1,* and TOPEX/Poseidon). The 1993 mean surface was calculated from *ERS-1* and TOPEX/Poseidon measurements. The monthly grids were computed by calculating a weighted average of crossover or collinear anomalies relative to 1993 reference surface. The data are evaluated on $1° \times 1°$ grid, with a search radius of 3° (Nerem et al. 1994). (The datasets and a description of the data processing can be found on the NASA Ocean Pathfinder project website at http://neptune.gsfc.nasa.gov/ocean/html)

A time–longitude section of the altimetric SSH anomaly gradient (not shown) indicates that the maximum anomaly in the North Atlantic appears in winter and spring every year, with the opposite signs before and after winter 1994/95. Therefore winter and spring data (December–February; March–May) are used to evaluate the SSH difference between the NAO positive and negative years. This SSH anomaly and the geostrophic current differences computed from the SSH are shown in Fig. 4b. One of the most pronounced features of this pattern is the general increase in meridional SSH gradient during the positive NAO winters, leading to the strengthening of the eastward flow near 50°N. The negative height anomaly in the northern portion of the basin has a minimum near 55°N, 40°E, indicating intensification of the cyclonic gyre in the Irminger Basin. The greatest intensification of the meridional velocities is observed in the northward flow along Rockall Trough. However, this anomalous flow does not appear to extend directly into the Nordic Seas, but instead turns slightly westward following topography and merges with the pronounced southeastward anomaly over the Iceland–Faeroe Ridge. An anomalous southward flow is observed during the NAO positive years in the Labrador Sea (Fig. 4b) and is probably related to the differences in ice cover between the two NAO phases.

The average geostrophic velocity differences between NAO positive and negative years inferred from the altimetric SSH measurements years are fairly small (on the order of 1 cm s^{-1}). The largest velocity differences (about 5 cm s^{-1} can be observed in the Gulf Stream (at 40°N, 60°W), in the southern and eastern part of the cyclonic gyre in the Irminger Basin (about 2–3 cm s^{-1}), over the Rockall Trough and in the Iceland–Faeroe Front (2 cm s^{-1}). These velocities are shown to be underestimates by a factor of 2–3 compared with drifter velocities, shown in the next section.

Because we next compare the circulation anomalies from the altimetry data with the flow from the Lagrangian drifters, we examine the consistency of the SSH disturbances compared with the NAO index during the 1992–98 period. Figures 7 and 8 show the time development of the most pronounced features of the difference between NAO positive and negative phases; that is, the flow in the cyclonic gyre in the Irminger Basin (Fig. 7) and the meridional flow in the easternmost (Rockall Trough) branch of the North Atlantic Current just west of Britain (Fig. 8). As indicated in Fig. 7a, the positive anomaly of zonal velocity in the Irminger gyre is largest in the winters of 1993/94 and 1994/95. The zonal velocity starts to decrease in 1996 and be-

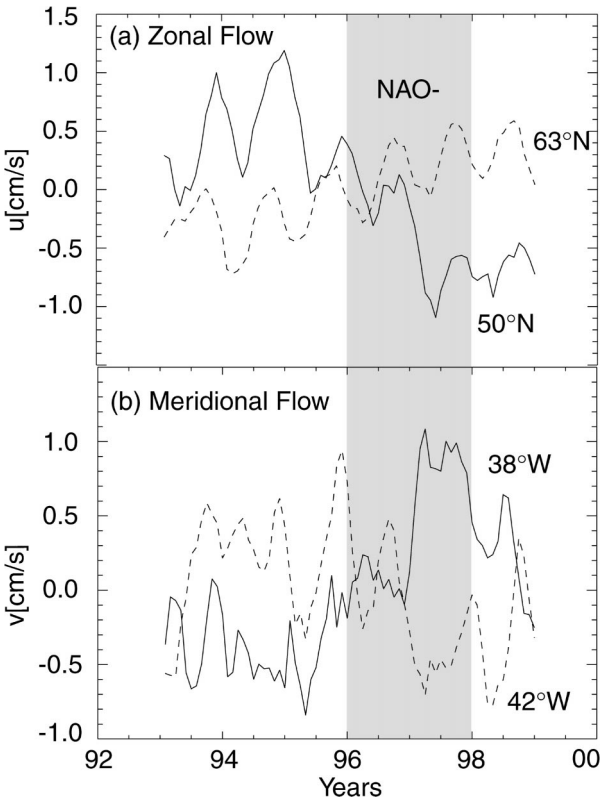

FIG. 7. (a) Zonal current anomaly (cm s^{-1}) at 50° and 63°N, evaluated at 38°W, and (b) meridional current anomaly (cm s^{-1}) at 38° and 42°W, evaluated at 56°N, from altimetry data.

comes negative in the following winters. The zonal velocity anomaly at 63°N increases steadily. This development results in a cyclonic anomaly before the 1995/96 switch and an anticyclonic anomaly afterwards. The meridional velocity anomalies (Fig. 7b) are consistent with this pattern. Northward anomalous flow at 38°W and southward anomalous flow at 42°W are observed before the switch, with the opposite pattern developing afterward. It is worth noting that the ocean circulation change is delayed by a few months relative to the NAO index. In the fall of 1995 the ocean circulation anomaly in the Irminger Basin is still cyclonic, but it switches to anticyclonic in the late spring, and becomes strongly anticyclonic in the following years.

As shown in Fig. 8, the meridional flow in the eastern boundary (Rockall Trough) branch of the North Atlantic Current decreased steadily until the winter of 1997/98, creating the anomaly observed in Fig. 4b. This development suggests that NAO-related surface circulation anomalies are not limited to the 1995 and 1996 winters when the greatest surface pressure anomalies are observed, but are present in the early 1990s and persist (with the opposite sign) for the years after the switch. Such development is consistent with the NAO index from multivariate analysis defining the 1996/97 and 1997/98 winters as negative NAO regimes. Therefore

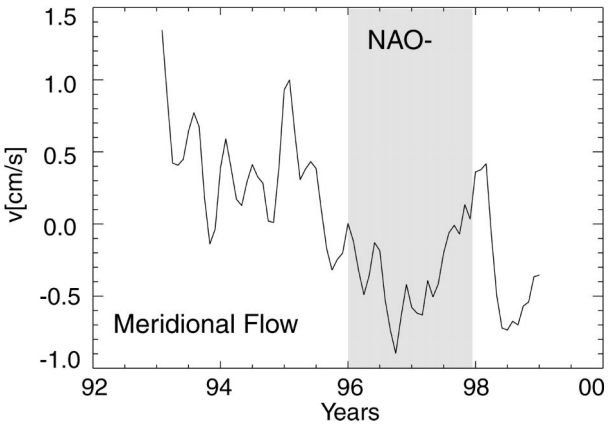

FIG. 8. The meridional current anomaly (cm s^{-1}) in the eastern (Rockall Trough) branch of the North Atlantic Current, at 55°N, 15°W, based on altimetry data.

it is reasonable to combine the drifter data for winters from 1992/93 to 1994/95 and from 1995/96 to 1997/98 to evaluate the difference in the surface currents during positive and negative NAO patterns.

c. NAO+/NAO− circulation changes based on the Lagrangian drifters

To examine the surface currents observed during positive and negative NAO years we average the drifter velocities for winter/spring 1992/93–1994/95 (positive NAO) and 1995/96–1997/98 (negative NAO). Although the NAO signal is most pronounced in winter, there are not enough drifter data in all winters to produce a good average. Since the altimetric signal of NAO persists through spring, spring drifter data are included in the averages here, which cover December through May. At grid points where no data were available for the winter–spring circulation for either NAO regime, we assumed the velocity to be equal to the average flow shown in Fig. 6. The velocity field was then smoothed using a five-point running filter in the zonal and meridional directions. Such smoothing removes the fine features of the flow but emphasizes the general character of the circulation changes, making the comparison with the smoothed SSH-derived geostrophic flow more natural. The results of this calculation are shown in Figs. 9a,b. A similar procedure was used to calculate average flow for winter (December–February) and summer (June–August), shown in Figs. 9c,d. Caution should be used in interpreting the figures in ice-covered regions.

As suggested by altimetry data, the general northeastward flow is stronger during the positive NAO years. The strengthening of the cyclonic gyre during those years is also evident. The difference between the flow related to the positive and negative NAO pattern is similar to the difference between the winter and summer flow (Figs. 9c,d). It appears that the stronger circulation that develops in winter became even more pronounced

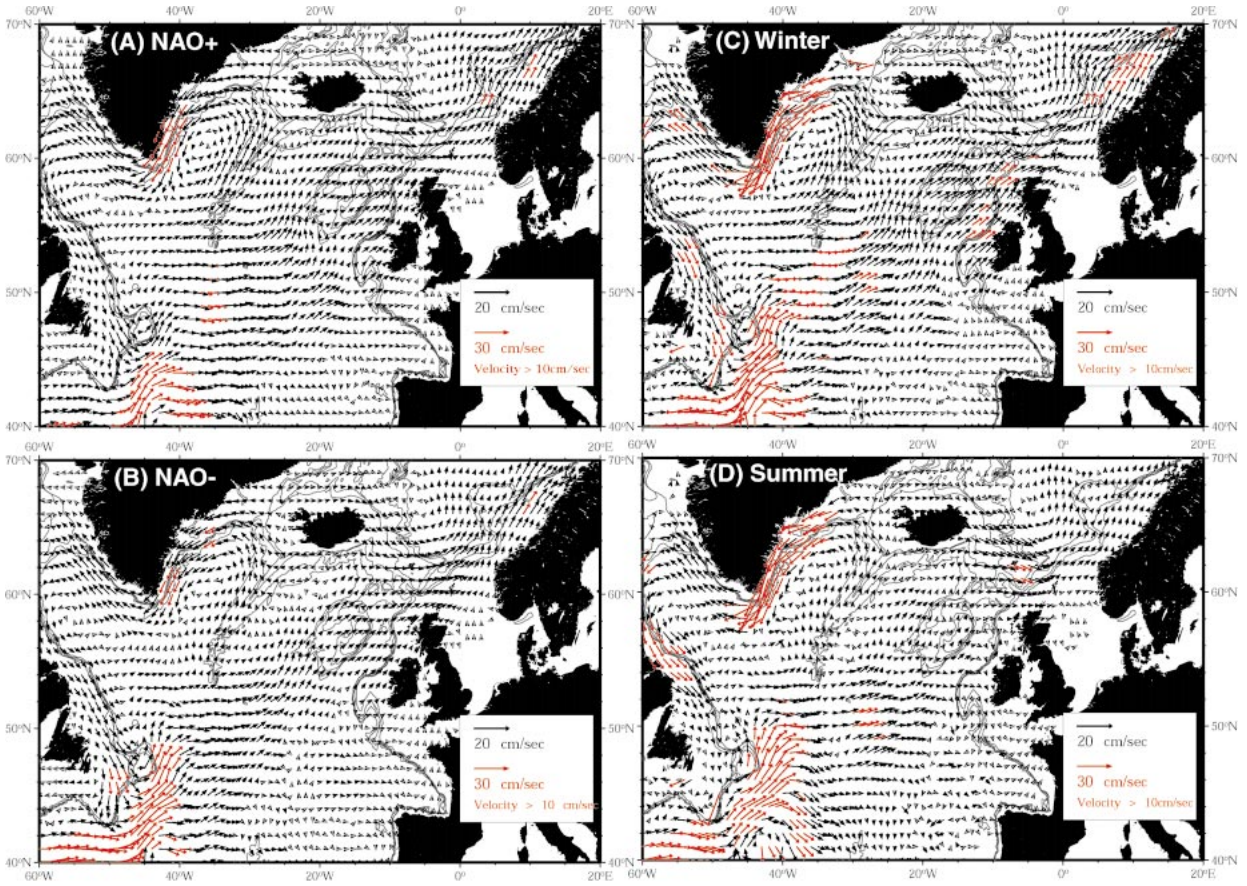

FIG. 9. Smoothed geostrophic velocity (cm s^{-1}) based on the drifters and Ekman velocities using NCEP winds for the (a) positive NAO winters (1992/93–1994/95) and (b) negative NAO winters (1995/96–1997/98). Data used are from winter and spring (Dec–May). The same for (c) winter (Dec–Feb) and (d) summer (Jun–Aug), averaged from 1992 to 1998.

during the NAO positive years. This is consistent with the atmospheric circulation patterns, where strong westerlies and low pressure in the Icelandic low present during winter become more pronounced in positive NAO years.

The difference between the positive and negative NAO surface velocity patterns is shown in Fig. 10. The drifter patterns are remarkably similar to the geostrophic flow anomaly pattern obtained from altimetry data, in spite of the fact that the circulation difference from drifters is based on a limited amount of data for each bin and required removal of the Ekman flow, which might not be completely modeled. At some grid points we had only one or two months of data for each NAO pattern. In both the altimetry and drifter datasets the strengthening of the eastward flow and cyclonic circulation in the Irminger Basin is evident. In addition, smaller-scale features observed in altimetry can also be detected in the drifter data. For example, there is an indication of the cyclonic anomalous flow related to the SSH maximum at the 52°N, 20°W. An eastward turn of the anomalous flow west of Ireland (55°N, 10°W) can be observed in both datasets. These features seem to be a manifestation of the intensification and southeastward shift of the current system during the positive NAO, and are consistent with the SST anomalies described in section 3d. The northward anomalous flow on the Newfoundland shelf suggests a strengthening of the southern portion of Labrador Current during the NAO negative years. The anomaly pattern in the northern part of the Labrador Sea seen in the drifters and altimetry indicates a southward shift of the Labrador Current during the NAO positive years, probably connected with variations in the ice cover (Deser et al. 2002).

The largest discrepancy between the altimetric and drifter geostrophic flows is in the Gulf Stream region. The drifters (Fig. 10) show large-scale anomalies with a large westward anomaly in the Gulf Stream west of 45°W, a southward anomaly in its branch into the western boundary portion of the North Atlantic Current, and an eastward anomaly in the eastward extension between 40° and 30°W. The altimetric differences on the other hand (Fig. 4b) show a series of alternating eddies of about 2° width. This difference is probably closely related to the sampling differences, as this is also the area where the error ellipses are large compared to the av-

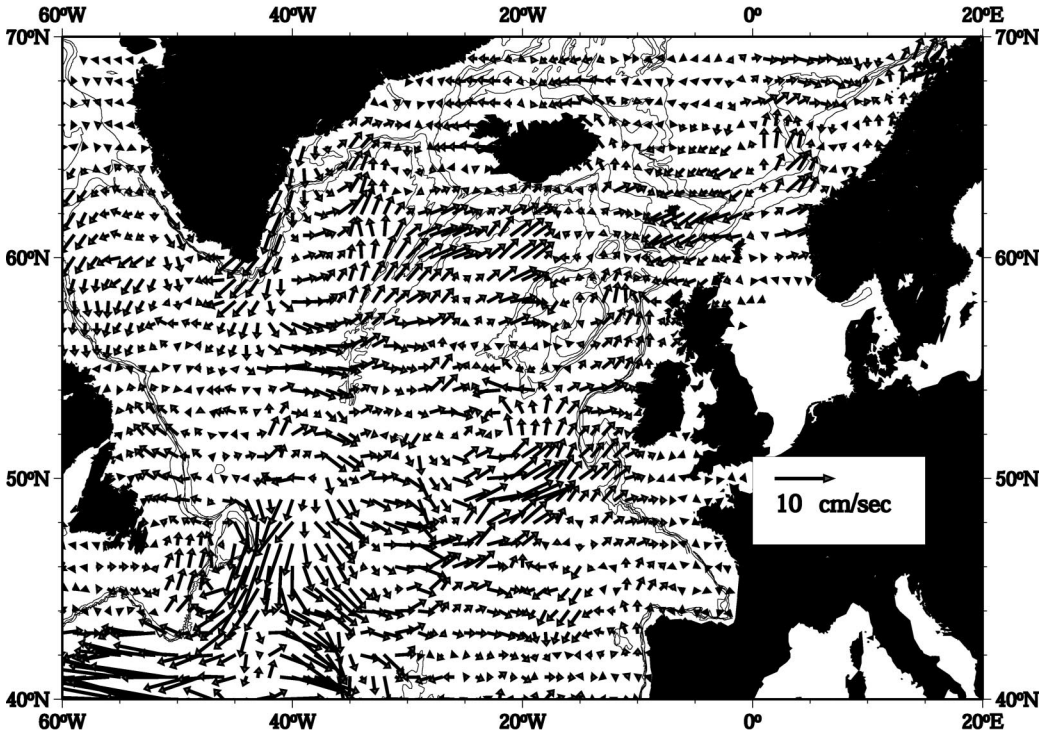

FIG. 10. Surface geostrophic velocity (cm s^{-1}) for positive NAO minus negative NAO years, calculated from the Lagrangian drifter velocities with Ekman velocities from NCEP winds. Data used are from winter and spring (Dec–May).

erage velocities. The large variance here is characteristic of the flow, and not a result of undersampling from the drifters, which are if anything more concentrated here than elsewhere.

Discrepancies in drifter and altimeter-based circulations around Iceland are also apparent. The drifters show a fairly large northeastward anomaly over the Reykjanes Ridge that does not appear in the SSH-derived flow. This anomaly is apparently due to a strengthening of both the Irminger Current and the Iceland Basin branch of the North Atlantic Current (subpolar front) during positive NAO years. Again, this is the area of large error-mean-flow ratio due to the presence of mesoscale eddies. North of Iceland, the drifters suggest weakening of the North Icelandic Current during the NAO positive years. Because of the lack of altimetry data in this region, this effect cannot be observed in SSH but, as we will show in the next section, it is consistent with SST patterns obtained from the AVHRR data.

The biggest difference in the two patterns lies in the magnitude of the geostrophic flow, with the flow observed by drifters about 2–3 times larger than SSH-derived velocities, in spite of the spatial smoothing used in deriving the positive–negative NAO difference from drifters shown in Fig. 10. The lower SSH-derived velocities may be related to large-scale smoothing of the altimetry to match along-track and cross-track sampling. As shown in Verbrugge and Reverdin (2003), whose velocities based on altimetry were similar in magnitude to those shown here, the choice of altimetry product can greatly affect the calculation of the geostrophic velocities. It is also possible that residual unremoved Ekman flow, resulting from inadequacies in the Ekman model, could contribute to the positive–negative NAO difference, especially near 55°N, 40°W, south of Iceland, and in the southern part of the Labrador Sea where the ratio of the Ekman to geostrophic component was relatively large (larger than 0.5).

d. Sea surface temperature, air–sea heat fluxes, and advective fluxes

The drifter velocity fields lend themselves to initial considerations of the possible role of advection in NAO-associated changes in sea surface temperature (SST) in the subpolar North Atlantic, as compared with surface heat fluxes. It has been shown (Hansen and Bezdek 1996) that SST anomalies created by the surface fluxes can be advected by the surface currents. Our analysis of Reynolds SST for the years 1992–99 (not shown here) indicates that a cold SST anomaly at 50°N (see Fig. 12a) associated with positive NAO developed in 1993 around 40°W and propagated eastward, until it was replaced by the warm anomaly in the winter of 1995/96, as shown previously by Deser et al. (2002). While we do not show details of this sort of propagation, we can show the pathways and size of advective heat flux during the two NAO regimes. We can also draw some qualitative con-

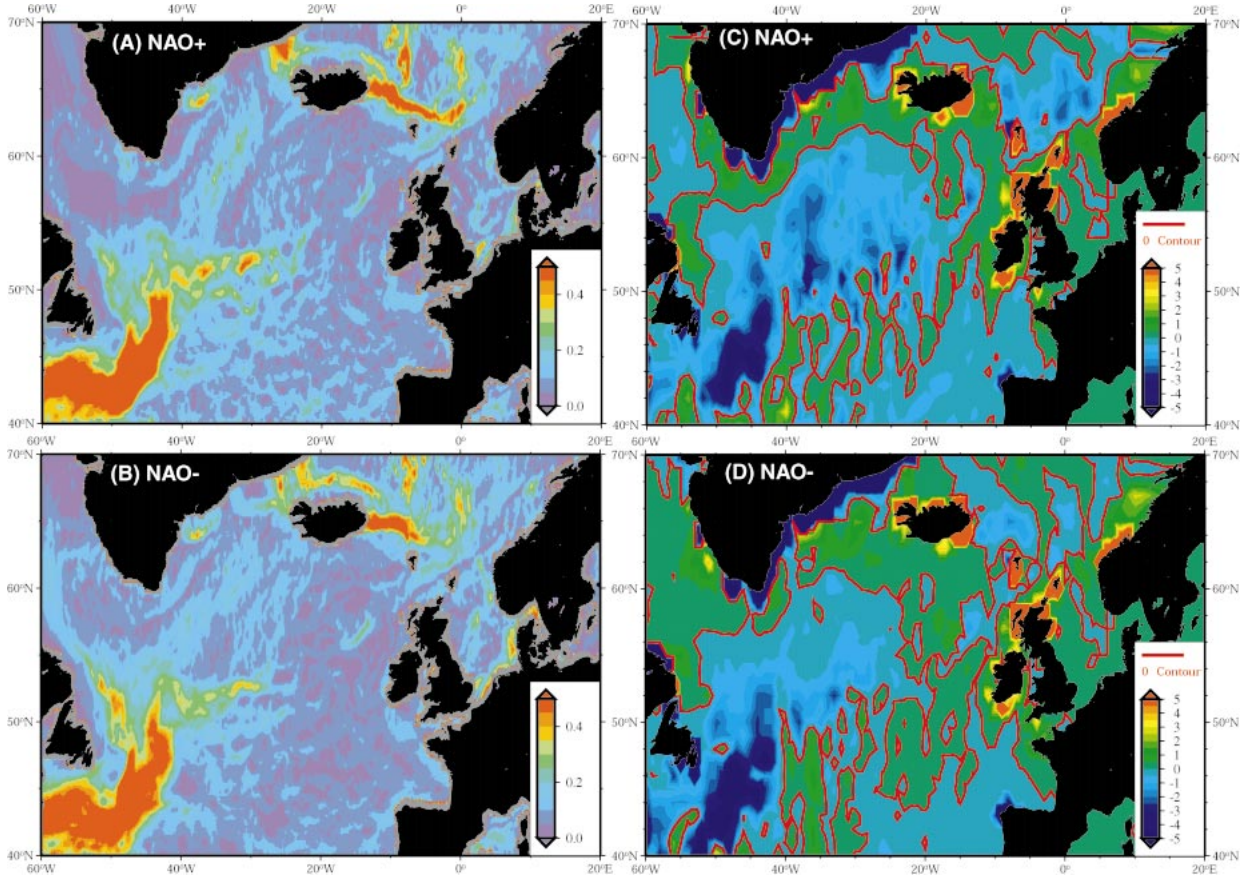

FIG. 11. (a),(b) Amplitude of the SST gradient (°C m^{-1}) from AVHRR data for positive and negative NAO winters/springs. Data used are Dec–Feb. (c), (d) Surface temperature advection (geostrophic plus Ekman) during the positive and negative NAO phase. The plotted value is $-\mathbf{u} \cdot \nabla T$ (°C month^{-1}), using the drifter velocities and AVHRR SST. Negative values indicate advective cooling (causing a drop in T). Data are from winter–spring (Dec–May).

clusions about the relative roles of air–sea flux and advection, particularly where interannual advection could be important. A complete analysis of the heat budget is beyond the scope of this paper, as we have not estimated variations in vertical distribution of air–sea heat flux, nor does drifter sampling resolution allow the full, say monthly, history of advection for careful consideration of advection versus heat fluxes in changing SST.

We show four products/calculations relevant to SST change: 1) SST gradients during each NAO phase (Figs. 11a,b); 2) horizontal advection during each NAO phase (Figs. 11c,d); 3) SST differences (Fig. 12a); and 4) air–sea heat flux differences (Fig. 12b). SST is obtained from AVHRR data. Horizontal advection flux is calculated using the drifter velocities and AVHRR SST. Air–sea fluxes are calculated from NCEP reanalysis products.

To look at the effects of SST advection during the different NAO phases, we examine the advective term $\mathbf{u} \cdot \nabla T$ estimated from the total (geostrophic plus Ekman) drifter velocities and AVHRR SST (Fig. 11). Since we do not have enough data to evaluate the velocity field for each year, currents and SST fields are both averaged for positive (1992/93–1994/95) and negative (1995/96–1997/98) winters. Therefore, this rough estimate likely underestimates the effects of short-lived strong anomalies in both SST and velocity fields that could develop in years with the very high or very low NAO index.

The SST advection ($-\mathbf{u} \cdot \nabla T$) tends to cool most of the central subpolar region (Figs. 11c,d). Examining the zonal and meridional components of the advective flux (not shown here) indicates that this is mainly due to the eastward advection of cold water across the subpolar front. The northward advection of the warmer waters tends to oppose this cooling but since the meridional component of advective flux has smaller magnitude, the total advection is dominated by the zonal effects. In both NAO phases, the axis of cooling is centered just north of 50°N, stretching northward to about 60°N. Maximum cooling is observed where the geostrophic flow of the North Atlantic Current is almost perpendicular to the surface isotherms. The maximum cooling rate is large: more than 3°C month^{-1}. Advective cooling is also found along and north of the Iceland–Faeroe Ridge and

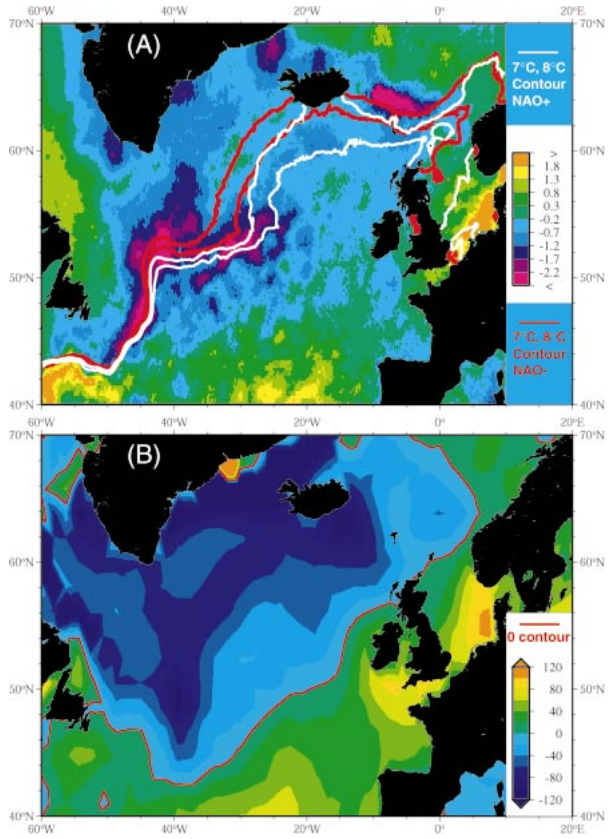

FIG. 12. (a) SST (°C) for NAO positive (1994/95) minus NAO negative (1995/96) winters, from AVHRR data. The red curves show the position of 7° and 8°C for the negative years; the black curves show the same for the positive years. (b) Total (latent plus sensible plus shortwave plus longwave) surface heat fluxes (W m^{-2}) for winter, 1994/95 minus winter, 1995/96, from NCEP reanalysis fluxes. Data used are Dec–Feb.

appears to be caused by the southward flow along the ridge.

South and east of the North Atlantic Current, relatively weak, advective warming occurs. Advective warming related to the westward flow crossing the Reykjanes Ridge is also observed in the northern part of the Irminger Basin and along the east coast of Greenland.

Analysis of the Ekman component of advection (not shown) indicates that the contribution of the Ekman flow is most significant east of the Flemish Cap and between 50° and 55°N, causing cooling due to southward Ekman advection in these areas. The Ekman cooling increases during the NAO positive years.

During positive NAO, when the winds and hence advection are stronger (Figs. 4 and 10), the advective cooling in the North Atlantic Current is intensified. Near the Iceland–Faeroe Front, the eastward flow in the North Icelandic Current is stronger during the negative NAO years, causing cold advection east of Iceland and contributing to the larger SST gradient observed in this area (Figs. 11a,b).

The SST gradient is part of the advective term of course, and the absolute value of the SST gradients (Figs. 11a,b) is of interest in itself. In both phases of the NAO, the highest gradients are associated with the Gulf Stream and North Atlantic Current Front, and with the Iceland–Faeroe Front and a front in the Denmark Strait. Relatively high SST gradients are also found through the Irminger Sea.

Changes in SST gradient between the positive and negative NAO phase agreed with the circulation changes observed with drifter data. The intensification of the eastward flow in the North Atlantic Current during the positive NAO winters corresponded to a sharper SST gradient at the subpolar front in this region. Similarly, the larger gradients that were observed in the cyclonic gyre in the Irminger Basin agreed with the stronger circulation that developed there in positive years. The SST gradient also supported our finding from drifter data of more intense flow around the northern coast of Iceland in the North Icelandic Current during the negative phase of NAO. During the positive phase, the warm anomaly northeast of Iceland weakened the SST gradient and at the same time the current velocities observed by drifters were smaller. North of the Faeroe Ridge, the stronger gradient east of the Faeroe Islands during the positive years agreed with the velocity anomaly calculated from the altimetry results. However, we were not able to observe these velocity changes in the drifter data.

The observed SST difference between negative and positive NAO (Fig. 12a) shows overall cooler SST in most of the subpolar region during positive NAO. This corresponds to an overall increased heat loss (Fig. 12b). In the Labrador Sea, the SST changes were of different sign in the West Greenland and Labrador Current regions (cooling and warming, respectively, in the positive NAO). The maximum warming region near the Labrador coast is a small area where the ice cover was smaller during the NAO positive years, in spite of a general increase of ice cover in surrounding regions. At the highest latitudes shown there was an SST decrease north of and parallel to the Iceland–Faeroe Ridge, and a warming north of this. High-latitude warming occurred north of Iceland near 70°N and 10°W; this pattern extended farther north but is not shown here. This Nordic Sea SST anomaly persisted from 1991 to 1995, decreased in 1996, and was replaced by a cold anomaly in 1997.

Change in air–sea heat flux (Fig. 12b) is associated with the very broadest scale of observed SST development (Fig. 12a). Changes in surface heat flux were most pronounced between the winters of 1994/95 and 1995/96. The whole northwestern part of the basin lost much more heat to the atmosphere during the 1994/95 winter (NAO positive), during which wind speeds were higher (Fig. 4a), than during the following winter (NAO negative). This pattern was associated with a broadscale warming after the NAO switch. The largest heat flux

differences (almost 100 W m^{-2}) are found in the broad northwestern region. The southern and eastern subpolar region lost less heat during the NAO positive winter, which is reflected in higher temperatures south of 45°N and in the shallow regions nearer the coast (North Sea, English Channel, etc.; Fig. 12a).

In the Nordic Seas, reduced heat loss in the winter of 1994/95, especially near 70°N, 10°W, was partially responsible for the positive SST anomaly in this area, but also requires advection. The smaller air–sea fluxes in the Nordic Seas during the positive NAO were the result of weaker and more southerly winds bringing warmer and moister air from the south. The largest heat flux difference between the NAO positive and negative phase was caused by variations in ice cover along the coast of Greenland. For example, while during the 1994/95 winter the area near the coast of Greenland was losing heat at about 300 W m^{-2}, the following year this flux was almost entirely eliminated by the expanding ice cover. The situation was reversed in the eastern Labrador Sea which, unlike the Greenland coast, had more extensive ice cover during the positive NAO.

The details of the patterns of SST and heat loss change differ significantly, in the sense of more enhanced SST change along the axis of the North Atlantic Current and Iceland–Faeroe Front compared with the broader, smoother, and northwestward-intensified heat loss pattern, associated with enhanced northwesterly winds (Fig. 4a). The most significant regional detail, unaccounted for by the surface heat loss, is the intensification, by up to −3°C, along the axis of the North Atlantic Current and north of the Greenland–Faeroe Ridge. The SST decrease also has an intensified axis into the Irminger Sea. The maximum change along the North Atlantic Current, at about 52°N, is located in the region of the most strengthened westerlies (Fig. 4a).

Since the air–sea heat flux does not account for the intensified SST change along the fronts, the change in SST advection (Figs. 11c,d) and a shift in the locations of the North Atlantic Current and Iceland–Faeroe Front must be responsible for cooling in this region. The 7° and 8°C isotherms are a rough indicator of the North Atlantic Current axis. They were displaced eastward during the NAO positive years, consistent with the shift of the subpolar front in the Icelandic Basin observed by Bersch et al. (1999) from hydrographic data.

Thus a dynamical change of the subpolar gyre, that is, a spinup of the circulation and eastward displacement of the North Atlantic Current front during the positive NAO phase, are most likely responsible for the intensified SST decrease through the middle of the region, along 52°N. Surface heat loss was larger during positive NAO, consistent with the stronger winds, and most likely was the cause of the broadscale SST decrease.

4. Summary and conclusions

We examined the interannual changes in the North Atlantic surface currents using Lagrangian drifters and associated datasets collected from 1992 to 1998. Since, at this time, several hundred buoys had been released in the Atlantic, the coverage of the area was good enough to evaluate the difference in circulation between the early 1990s, which were dominated by the positive NAO pattern and the winter of 1995/96 and the following two winters where the pattern was predominantly negative. Positive NAO years referred to the winters 1992/93–1994/95 and negative NAO years referred to winters 1995/96–1997/98 in the preceding sections. This is a fairly short time period, and although we hope this analysis will help us to understand the long-term effects of NAO, many circulation features have longer timescales and are not completely represented here.

Our analysis indicates that the interannual changes observed in the drifter data were similar in pattern to the seasonal variability, with the enhanced winter characteristics of the flow observed during the NAO positive years. The variability of the surface currents observed with drifter data was supported by the changes in the geostrophic flow calculated from the altimetric SSH data, although the magnitude of the variability was about 2–3 times larger in the smoothed drifter data results than in the altimetric results.

The most pronounced circulation changes observed in the drifters and altimetry are the intensification of the northeastward flow throughout the basin and intensification of the cyclonic circulation in the Irminger Basin during the positive phase of NAO. These changes, coupled with SST temperature anomalies influence the SST distribution and could thus affect air–sea interaction.

Acknowledgments. This study was supported by the National Science Foundation Ocean Sciences Division through Grant OCE-9529584 as part of the Atlantic Climate Change Experiment component of the World Ocean Circulation Experiment. Drifter observations and analyses in the North Atlantic were supported by the NOAA Office of Global Programs.

REFERENCES

Barnston, A., and R. Livezey, 1987: Classification, seasonality and persistence of low-frequency atmospheric circulation patterns. *Mon. Wea. Rev.,* **115,** 1083–1126.

Bersch, M., J. Meincke, and A. Sy, 1999: Interannual thermohaline changes in the northern North Atlantic 1991–1996. *Deep-Sea Res.,* **46,** 55–75.

Bower, A., and Coauthors, 2002: Directly measured mid-depth circulation in the northeastern North Atlantic Ocean. *Nature,* **419** (6907), 603–607.

Cayan, D., 1992: Latent and sensible heat flux anomalies over the northern oceans: Driving the sea surface temperature. *J. Phys. Oceanogr.,* **22,** 859–881.

Czaja, A., and C. Frankignoul, 1999: Influence of the North Atlantic SST on the atmospheric circulation. *Geophys. Res. Lett.,* **26,** 2969–2972.

Deser, C., M. Holland, G. Reverdin, and M. Timlin, 2002: Decadal variations in Labrador sea ice cover and North Atlantic sea surface temperatures. *J. Geophys. Res.,* **107,** 3035, doi:10.1029/2000JC000683.

Dietrich, G., K. Kalle, W. Krauss, and G. Siedler, 1975: *Allgemeine Meereskunde.* 3d ed. Borntraeger, 628 pp.

Fratantoni, D. M., 2001: North Atlantic surface circulation during the 1990s observed with satellite-tracked drifters. *J. Geophys. Res.,* **106** (C10), 22 067–22 093.

Hansen, D., and H. Bezdek, 1996: On the nature of decadal anomalies in North Atlantic sea surface temperature. *J. Geophys. Res.,* **101,** 8749–8758.

——, and P. Poulain, 1996: Quality control and interpolation of WOCE/TOGA drifter data. *J. Atmos. Oceanic Technol.,* **13,** 900–909.

Hurrell, J., 1995: Decadal trends in the North Atlantic Oscillation: Regional temperatures and precipitation. *Science,* **269,** 676–679.

Joyce, T., C. Deser, and M. Spall, 2000: The relation between decadal variability of subtropical mode water and the North Atlantic Oscillation. *J. Climate,* **13,** 2550–2569.

Krauss, W., 1986: The North Atlantic Current. *J. Geophys. Res.,* **91** (C4), 5061–5074.

——, 1995: Currents and mixing in the Irminger Sea and in the Iceland basin. *J. Geophys. Res.,* **100** (C6), 10 851–10 871.

Lavender, K., H. Davis, and W. Owens, 2000: Mid-depth recirculation observed in the interior Labrador and Irminger Seas by direct velocity measurements. *Nature,* **407,** 66–69.

McClean, J. L., P. M. Poulain, J. W. Pelton, and M. E. Maltrud, 2002: Eulerian and lagrangian statistics from surface drifters and a high-resolution POP simulation in the North Atlantic. *J. Phys. Oceanogr.,* **32,** 2472–2491.

Mysak, L., and S. Venegas, 1998: Decadal climate oscillations in the Arctic: A new feedback loop for atmosphere–ice–ocean interactions. *Geophys. Res. Lett.,* **25,** 3607–3610.

Nerem, R., E. Schrama, C. Koblinsky, and B. Beckley, 1994: A preliminary evaluation of ocean topography from the TOPEX/POSEIDON mission. *J. Geophys. Res.,* **99,** 24 565–24 583.

Olbers, D. J., M. Wenzel, and J. Willebrand, 1985: The inference of North Atlantic circulation patterns from climatological hydrographic data. *Rev. Geophys.,* **23** (4), 313–356.

Orvik, K. A., O. Skagseth, and M. Mork, 2001: Atlantic inflow to the Nordic Seas: Current structure and volume fluxes from moored current meters, VM-ADCP, and SeaSoar-CTD observations, 1995–1999. *Deep-Sea Res.,* **48** (4), 937–957.

Pazan, S., and P. P. Niiler, 2001: Recovery of near-surface velocity from undrogued drifters. *J. Atmos. Oceanic Technol.,* **18,** 476–489.

Poulain, P.-M., A. Warn-Varnas, and P. P. Niiler, 1996: Near-surface circulation of the Nordic Seas as measured by Lagrangian drifters. *J. Geophys. Res.,* **101** (C8), 18 237–18 258.

Ralph, E., and P. Niiler, 1999: Wind-driven currents in the tropical Pacific. *J. Phys. Oceanogr.,* **29,** 2121–2129.

Reid, J. L., 1994: On the total geostrophic circulation of the North Atlantic Ocean: Flow patterns, tracers and transports. *Progress in Oceanography,* Vol. 33, Pergamon, 1–92.

Reverdin, G., N. Verbrugge, and H. Valdimarsson, 1999: Upper ocean variability between Iceland and Newfoundland, 1993–1998. *J. Geophys. Res.,* **104,** 29 599–29 611.

Schmitz, W. J., and M. S. McCartney, 1993: On the North Atlantic circulation. *Rev. Geophys.,* **31,** 29–49.

Stommel, H., P. Niiler, and D. Anati, 1978: Dynamic topography and recirculation of the North Atlantic. *J. Mar. Res.,* **36,** 449–468.

Sutton, R., and M. Allen, 1997: Decadal predictability of North Atlantic sea surface temperature and climate. *Nature,* **388,** 563–567.

Sverdrup, H. U., M. W. Johnson, and R. H. Fleming, 1942: *The Oceans: Their Physics, Chemistry and General Biology.* Prentice-Hall, 1086 pp.

Thompson, D., and J. Wallace, 1998: The Arctic Oscillation signature in the wintertime geopotential height and temperature fields. *Geophys. Res. Lett.,* **25,** 1297–1300.

——, ——, and G. Hegerl, 2000: Annular modes in the extratropical circulation. II. Trends. *J. Climate,* **13,** 1018–1036.

Verbrugge, N., and G. Reverdin, 2003: Contribution of horizontal advection to the interannual variability of sea surface temperature in the North Atlantic. *J. Phys. Oceanogr.,* **33,** 964–978.